THERMAL FATIGUE DISLOCATION STRUCTURES IN 316L STEEL: EXPERIMENTS AND SIMULATIONS

C.F. Robertson[1] M.C. Fivel[2] and A. Fissolo[1]

[1] SRMA CEA/Saclay, 91191 Gif-sur-Yvette, France.
[2] GPM2 CNRS/INPG, BP 46, Domaine Universitaire, 38402 Grenoble, France.

ABSTRACT

In an attempt to better understand damage accumulation mechanisms in thermal fatigue, dislocation substructures forming in 316L steel during a specific test are examined and simulated. Hence, thin foils taken out of massive, tested specimens are observed in transmission electron microscopy (TEM). These observations help in determining an initial dislocation configuration to be implemented in a 3D model combining 3D discrete dislocation dynamics simulation (DDD) and finite element method computations (FEM). It is found that the simulated mechanical behaviour of the DDD microstructure is compatible with FEM and experimental data. The numerically generated dislocation microstructure is similar to ladder-like dislocation arrangements as found in many fatigued f.c.c. materials. Distinct mechanical behaviour for the two active slip systems are shown and deformation mechanisms are proposed. Up to T=650K, no evidence for direct effect of temperature on climb and cross slip phenomenon was found.

KEYWORDS

Multiscale Modelling, 3D Discrete Dislocation Simulation, Fatigue Simulations, TEM, FEM.

INTRODUCTION

Thermal fatigue in the temperature range 300K-700K constitutes typical loading conditions for metallic pressure vessels and piping used in the electric power industry [1]. In these conditions, component material failure results from transgranular crack initiation and propagation [2], regardless of the component surface state finish [3]. Transgranular cracking therefore results from damage accumulation mechanisms operating at a scale much smaller than the metal grain size. Hence, little is known about dislocation based, mesoscopic scale deformation mechanisms in component materials undergoing thermal fatigue. In an attempt to better understand phenomenon involved in thermal induced cyclic plasticity, an innovative investigation approach is proposed here and adapted to a widely used component material, 316L austenitic stainless steel (f.c.c. crystalline structure).

One ‘classical’ tool to investigate fatigue dislocation substructure is the transmission electron microscopy (TEM) technique [4-8]. Though informative, TEM examinations are very difficult to rationalise in terms of dynamic deformation mechanisms, due to the very large number of dislocations involved. In addition, it is very difficult to establish how the identified mechanisms influence larger-scale mechanical behaviour. One way to cope with these problems is to use numerical modelling that couples information coming from different scales. Modelling reliability can then be established by direct comparisons of numerical results with adequate experimental data. In the present paper, dislocation substructures forming in 316L steel during a

specific test are examined and simulated in order to better understand damage accumulation mechanisms in thermal fatigue. In the next sections, we will describe in detail both the selected experimental setting (thermal fatigue tests, TEM) and the proposed numerical methods (discrete dislocation dynamics, finite element method). In the next section, an application of these methods to a specific thermal fatigue test will be presented and the results given. Information coming out of the proposed approach is summed up in a brief conclusion.

EXPERIMENTS

Thermal fatigue tests

The experimental apparatus is presented in Figure 1(a). Specimens are machined from plates in the solution annealed state. The mean grain size is about 50µm. Portions of the external wall will be extracted after fatigue test for TEM examination. These portions are electropolished before testing. This eliminates any residual plastic deformation that can affects the interpretation of the results. During the test, the external specimen surface is heated by HF induction while the internal surface is continuously cooled by flowing water. This gives rise to a radial temperature gradient between the two walls, enforcing a thermal-induced stress field. Fatigue loading conditions are achieved by switching the heating on and off periodically ($f \approx 8\times10^{-3}$ Hz), up to 100 cycles. In these conditions, temperature of the internal wall fluctuates from 22°C to 80°C during the cycle, whereas temperatures of the external wall varies between 32°C and 380°C.

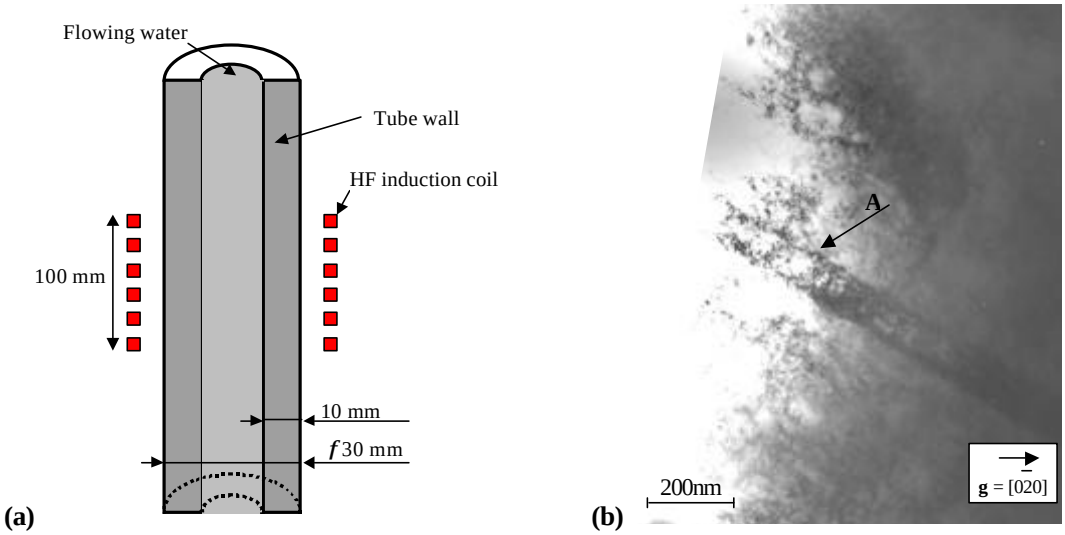

Figure 1: (a)-Experimental apparatus. **(b)**-TEM observation of a surface grain

TEM observations

After test, 2cm×1cm×0.1cm slices from (the electropolished) parts of the external wall surface are cut out of the massive tube specimens, using a rotating precision saw. These slices are further thinned to 100µm by mechanically polishing the back. Then, 3mm disks are punched out. TEM thin foils are prepared using back side electropolishing in a twin jet Tenupol, while the external surface is protected by lacquer. The TEM observations are then made in a CM-20 Philips operated at 200kV.

Out of the observed specimens, a single grain has been selected for a complete indexation, with a view to use these results for DDD simulations. According to electron diffraction pattern analysis, the observed grain plane (the TEM foil top surface) is found to be close to (211).

In Figure 1(b), a pair of 30nm thick parallel bands separated by a 100nm wide channel is shown (letter A). The channel is partially filled with dislocation lines more or less perpendicular to the bands, that are obviously parallel to $(\bar{1}11)$ planes. Using the **g.b** = 0 rule, it is found that band and channel dislocations share the same Burgers vector ½[110]. The two possible active slip systems for dislocations present in and between these bands are thus $(\bar{1}11)$ [110] and $(1\bar{1}1)$ [110].

MODELLING

Finite element method (FEM) computations

Strain and stress fields generated during test are computed by FEM, using CASTEM-2000 software. By taking advantage of specimen geometry, the problem corresponding to the experimental setting as shown in Figure 1(a) can be solved with a mesh corresponding to one eighth of the specimen. Eight node cubic elements were used with a mean element width of about 175 µm (see Figure 2(a)). Calculations were done as follows. Experimentally obtained temperatures in specimen internal and external walls are first imposed to the nodes corresponding to these respective walls. Temperature of every node inside the meshing is then computed assuming thermal equilibrium and the mentioned thermal boundary conditions. In the next computing step, the 'complete' thermal field together with suitable mechanical boundary conditions enforce a thermal induced displacement field. Associated strain and stress fields are computed assuming an elastoplastic model involving a linear kinematic yielding criteria that fits experimental fatigue data. Stresses estimated with this model agree with experimental saturation values at 300K.

FEM computations gives an equibiaxial thermal induced stress state ($\sigma_{zz} = \sigma_{\theta\theta} = \sigma$) which is in good agreement with analytical expressions found by Fissolo [2]. The stress amplitude is σ = -230MPa when T = T_{max} and σ = 130MPa when T = T_{min}. These conditions are often referred to as 'out of phase' thermal fatigue, i.e. the compressive stress (negative) peaks whereas the temperature is maximal. The mechanical stress-strain curve is plotted in Figure 2(b), for the zz components.

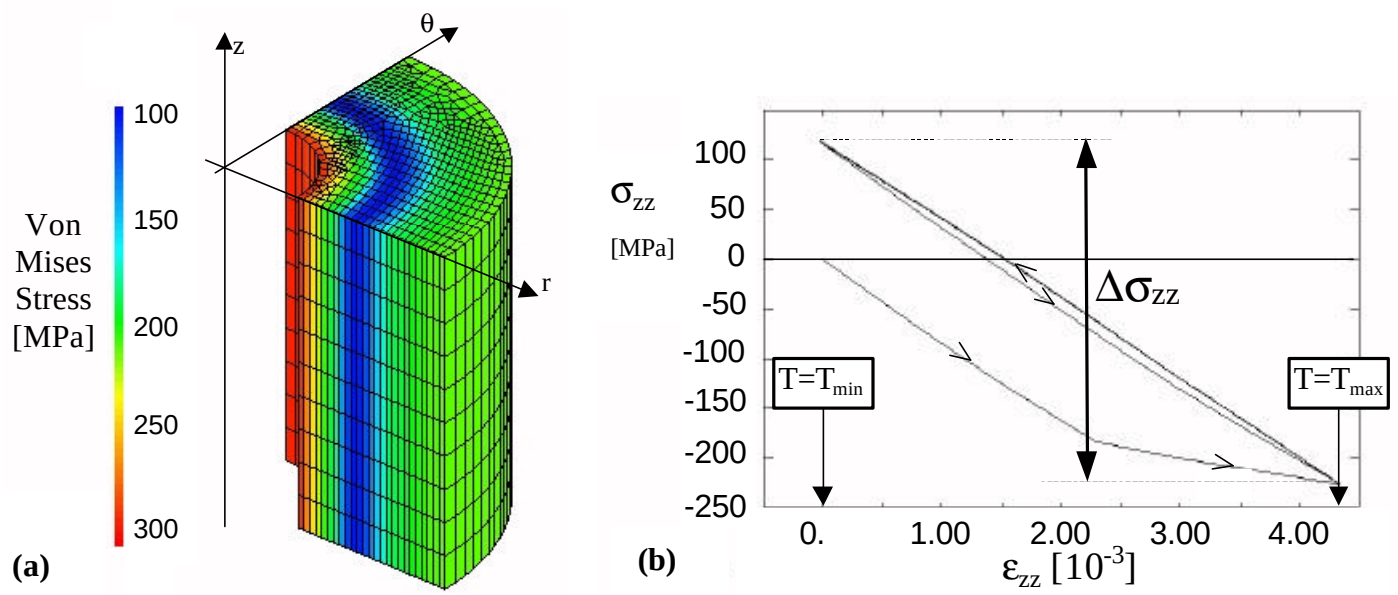

Figure 2: (a)-FEM Von Mises equivalent stress in MPa at maximal temperature T = 653K. The represented mesh corresponds to the part of the specimen located inside the induction coil described in Figure 1(a). Note that the external wall undergoes compressive stress whereas the internal wall is in tension.
(b)-External wall total loading (mechanical+thermal): $\sigma_{zz}(\varepsilon_{zz})$.

The resolved shear stress τ_R are then computed on all the 12 f.c.c. glide system of the grain identified in previous section. It is worth mentioning that $|\tau_R|$ on the $(\bar{1}11)[110]$ and $(1\bar{1}1)[110]$ slip systems (those of the identified 2D bands) are very similar, a condition we will later refer to as 'double' slip.

Discrete dislocation dynamics (DDD) simulation

The constitutive principles of DDD modelling are described in details elsewhere [10]. Numerically generated dislocations inside the simulation box glide in a homothetic 3D f.c.c. lattice, with a lattice parameter of 10b (2.5×10^{-9}m), where b is the Burgers vector magnitude. The dislocation lines are discretisized in screw and edge segments, whose displacement occurs over discrete time steps. For each time step, the effective resolved shear stress acting on all the segments are computed. Each segment is then moving at a velocity proportional to the effective stress. The DDD code treats all the possible 3D

annihilation/recombination interactions between the dislocations. A stochastic temperature-dependant cross-slip mechanism is implemented as well.

We will now attempt to simulate the dynamic evolution under cyclic thermal load of the same dislocation band pair as the one described in first section. The DDD simulation box is taken as a faceted cylinder with a selected radius and height of 5µm. The simulation box size is chosen so as to be similar to the experimentally observed separation distance between the selected pair of bands and the pair next to it (2µm). This box represents a part of a 316L grain, with upper and bottom faces parallel to (211) planes. Dislocations that reach the bottom and peripheral cylinder faces are stopped, producing strong barrier effects like dense dislocation walls and/or highly disoriented grain boundaries. The effect of the free surface is accounted for by allowing dislocations reaching the upper face to escape. The initial dislocation microstructure consists of 2 µm long pinned dislocation segments randomly put in the $(\bar{1}11)[110]$ slip system only (43 segments in all), which will be referred to as the primary slip system. Each pinned segment acts as a Frank-Read source with random sign and orientation. The initial sources are positioned at random inside two 30nm wide parallel bands centred in the simulation box and separated by a 100nm wide channel. This initial dislocation microstructure is selected in order to quickly obtain a configuration complying with TEM observations thus, with a known number of cycles N = 100. Of course then, this initial DDD dislocation configuration does not correspond to the microstructure of cycle N = 0 of the performed test, but instead to the N^{th} cycle, with $0 < N < 100$.

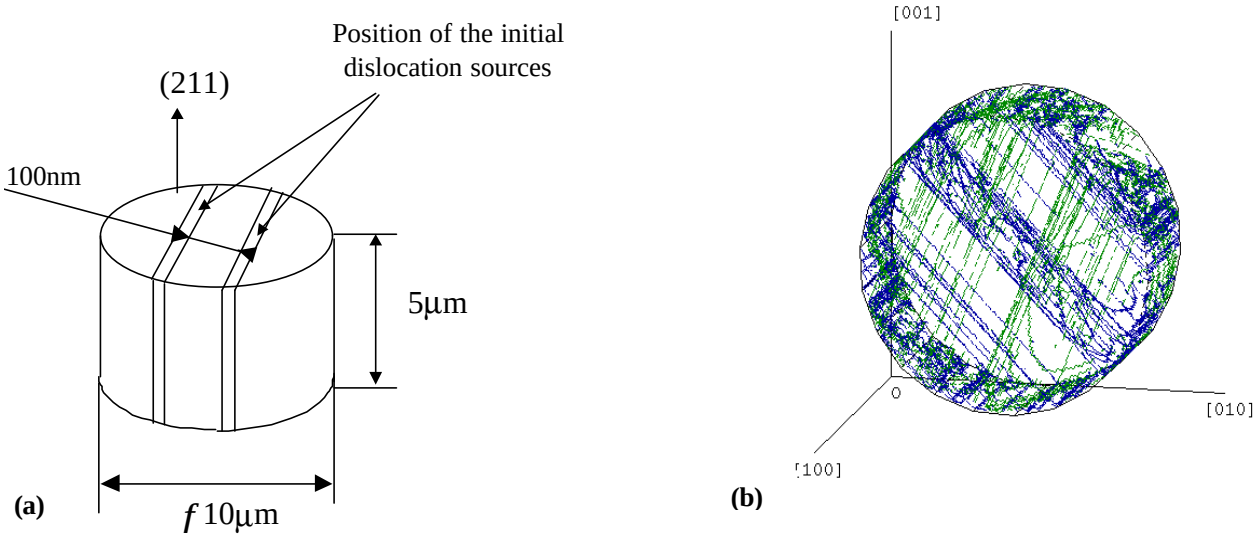

Figure 3: (a)-Schematic representation of the initial dislocation structure. **(b)**-3D dislocation microstructure obtained after 3 simulated cycles.

The numerical fatigue test is performed in imposed applied stress conditions. The *applied* stress field is as determined with the help of FEM computations. This field is assumed to be homogenous inside the whole simulation box, i.e. the same applied stress tensor is used for each dislocation segment. Note that although the applied stress field is homogeneous, the effective stress tensor computed at the middle point of each dislocation segment is heterogeneous due to the contribution of the internal stress field generated by the dislocation segments. In practice, the loading is enforced stepwise, 5MPa by 5MPa. Each time the applied load is changed, dislocations move and multiply over as many computing steps (with $\delta t=10^{-9}$sec) as needed to obtain a stable dislocation configuration, i.e. one that equilibrates the applied load. Therefore, as many as 460MPa/5MPa = 92 stable dislocation configurations have to be determined for each complete thermal cycle. Because one thermal cycle lasts 120 seconds, each stepwise load increase correspond to 120s/92 ~1.3 seconds. As dislocations move much faster than the applied load increase rate, equilibrium is usually achieved within as few as $N = 10^2$-10^3 time steps, i.e. $N\delta t \sim 10^{-7}$-10^{-6} seconds. At this point, if dislocation climb is neglected, cross slip is the only time-dependant mechanism that can further affect the microstructure inside the simulation box. This means that quasi-static approximation can here be fully assumed provided no more cross slip occurs within the ~1.3 second following stabilisation. This assumption has been checked in a separate paper [11]. Hence, the simulated time can here be converted into an equivalent time corresponding to the actual test duration.

Results

When the initial dislocation sources are placed inside the simulation box and applied load gradually increases, dislocation density in the primary slip system increases smoothly as shown in Figure 4(a). This regime lasts for the first half of the first simulated cycle, i.e. until $T = T_{max}$. At this point, the dislocation density in the deviate slip system (we recall that $\rho_{(t=0)} = 0$ in this slip system) starts increasing due to intense cross slip, until it is about half as large as in the primary slip system.

Over the last simulated applied cycle (third one), the equivalent mechanical strain of the simulation attains $\Delta\varepsilon_{eq} \sim 2\times10^{-3}$. Average dislocation density during that same cycle is around $\sim5\times10^{12}$ m^{-2}. By comparison, the equivalent mechanical FEM strain amplitude is $\Delta\varepsilon_{eq} \sim 2.2\times10^{-3}$ when the thermal expansion contribution is subtracted. However, it seems quite obvious that the straining is not homogeneous inside the simulation box. This is reflected by the heterogeneity of the dislocation densities. For example, the dislocation density computed inside a sphere of radius 500nm located inside the central bands is $\rho\approx5.4\times10^{13}$ m^{-2}. If that same sphere is now positioned outside the bands, the density ρ is reduced down to 7.9×10^{12} m^{-2}. At this stage thus, the DDD strain amplitude reasonably agrees with elastoplastic FEM results although a simplified model has been used: only 2 glide systems are considered, the influence of the image forces is neglected and no internal obstacles such as local twins or misorientation are taken into account. In a forthcoming study, all these points will be implemented and tested.

Interestingly, the mechanical behaviour of the two involved slip systems presents distinct characteristics, as plotted in Figure 4(b). Shear strain γ in the deviate slip system $(1\bar{1}1)[110]$ is periodic and vanishes one time per cycle. It is worth mentioning that a $\gamma = 0$ strain is associated with a non-vanishing dislocation density. This means that dislocations in this system can arrange in low shear strain configurations with a strongly reversible character.

In the primary slip system $(\bar{1}11)[110]$, shear strain accumulates from one cycle to an other, i.e. it is not fully reversible. In addition, dislocation density in the primary slip system is about twice that in the secondary slip system, whereas shear strain associated with the later is three times higher than that associated with the former. Hence, by opposition with the secondary system, the dislocation arrangements in the primary slip system maximize the induced shear strain.

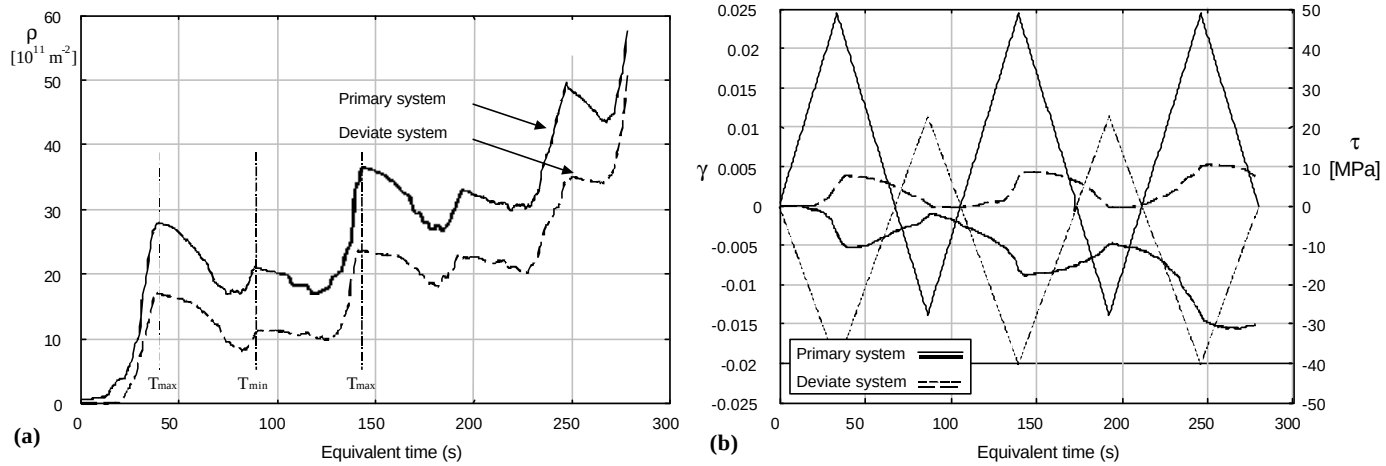

Figure 4: (a)-Dislocation density evolution ρ(time) on primary and deviate slip systems versus time. The plotted densities are associated with the whole simulation box. Local dislocations densities can be much higher. **(b)** Shear strain (left axis–thick lines) and applied shear stress triangular wave (right axis–thin lines).

Incidentally, most of the $(1\bar{1}1)$ slip planes do not cross the crystal top surface whereas dislocations present in these planes keep gliding there until they form stable, low energy dislocation substructures. Indeed, the $(1\bar{1}1)[110]$ dislocations located inside the channel between the two initial bands have a strong edge-edge dipolar character. Dynamic 'in test' observations show dipoles to form in large numbers as soon as the first applied load reversal begins. Obviously though, the cyclic character of the applied load strongly increases the dipole formation probability. Once an isolated dipole has formed, it promotes further dipole formation by capturing additional isolated dislocations. When a few dipole clusters have formed, they rearrange in

dislocation walls perpendicular to the **b** vector [110] common to primary and deviate slip systems, as soon as the applied stress becomes low enough. Secondary dislocations therefore tend to stabilise the primary walls substructure at this particular stage of the cycling. We assume that a secondary wall exists whenever at least 2 dipoles are positioned along $[1\bar{1}2]$ direction, inside each 500nm thick (211) slice cut out of the simulation box. Using this criteria, an average wall-wall separation of 250nm is measured. Note that dipole width inside the bands is more or less constant: isolated dipole width distribution is similar to that of dipoles everywhere else in the central bands.

It is worth mentioning that during the presented simulations, new bands spontaneously form at some distance (up to 1,5 µm) from the initial pair position. The new band formation occurs when screw dislocations located in some $(1\bar{1}1)$ planes (located out of the initial band pair) cross-slip back into some distant $(\bar{1}11)$ planes, near the simulation box edges. Obviously, this band formation mechanism is promoted under the present 'double' slip loading conditions. New band formation can also be assisted by the stress field coming from the accumulated dislocations at the simulation box edges thus, by the presence of a strong barrier.

CONCLUDING REMARKS

Although the present approach seems promising, many remaining questions have to be addressed. For example, how does the simulation box size affects the results? Here, the simulation box size has been chosen according to TEM observed minimal separation distance between two pairs of bands. The boundary conditions in the simulation box do not account for the actual grain boundary in the metal. This could be done by calculating more accurately the stress fields existing inside the grain.

In addition, the top surface of the simulation box, i.e. the external wall of the tested specimen, was not treated in a realistic way: dislocation segments crossing the surface were cut away. A specific treatment of the boundary conditions relevant to the presence of an oxide layer and/or a traction free surface has to be implemented.

Finally, due to the very large computing time, only about 3 cycles have been simulated. The stability of the results with time could be addressed. Therefore improved DDD algorithms have to be developed.

ACKNOWLEDGEMENTS

Authors wish to thank Mr. F. Bouchet for the skilful experimental work and acknowledge Dr. L. Boulanger, Dr. G. Martin and S. Poissonnet for their helpful suggestions and commentaries.

REFERENCES

1. Sehitoglu, H., ASM Handbook (1996). Vol.19 Fatigue and Fracture, Thermal and Thermomechanical Fatigue of Structural Alloys.
2. Fissolo, A., Marini, B., Wident, P. and Nais, G. (1994) *Soc. Fr. Métall. Matér*., pp. 513-526.
3. Wareing, J. and Vaughan, H.G. (1979) *Metal Science*, pp. 1-8.
4. Boulanger, L., Bisson, A. and Tavassoli, A.A. (1985) *Phil. Mag A*, 51(2), L5-L11.
5. Obrtlik, K., Kruml, T. and Polak, J. (1994) *Mat. Sci. Eng.* A187, 1.
6. Tavassoli, A.A. (1986) *Phil. Mag A* 54(4), 521.
7. Armas, A.F., Alvarez-Armas, I. and Petersen, C. (1992) *J. Nucl. Mat.* 191-194, 672.
8. Gerland, M., Mendez, J., Violan, P. and Ait Saadi, B. (1989) *Mat. Sc. Eng.* A118, 83.
9. Fissolo, A., Marini, B., Nais., G. and Wident, P. (1996) *J. Nucl. Mat.*, 233-237, 233.
10. Verdier, M., Fivel, M. and Groma, I. (1998) *Modelling Simul. Mater Sci. Eng*., 6(6), 755.
11. Robertson, C., Fivel, M.C. and Fissolo, A., *Mater. Sci. Eng A.*, in press.